Genetically Encoded Forster Resonance Energy Transfer-Based Biosensors Studied on the Single-Molecule Level

Hoefig, Henning; Otten, Julia; Steffen, Victoria; Pohl, Martina; Boersma, Arnold J.; Fitter, Joerg

Published in:
ACS Sensors

DOI:
10.1021/acssensors.8b00143

Publication date:
2018

ACS SENSORS

Article

Cite This: ACS Sens. 2018, 3, 1462−1470

pubs.acs.org/acssensors

Genetically Encoded Förster Resonance Energy Transfer-Based Biosensors Studied on the Single-Molecule Level

Henning Höfig,[†,‡] Julia Otten,[§] Victoria Steffen,[§] Martina Pohl,[§] Arnold J. Boersma,[∥] and Jörg Fitter*[,†,‡]

[†]I. Physikalisches Institut (IA), RWTH Aachen, 52074 Aachen, Germany

[‡]ICS-5: Molecular Biophysics, Forschungszentrum Jülich, 52425 Jülich, Germany

[§]IBG-1: Biotechnology, Forschungszentrum Jülich, 52425 Jülich, Germany

[∥]Groningen Biomolecular Sciences and Biotechnology Institute, University of Groningen, 9700 AB Groningen, Netherlands

Supporting Information

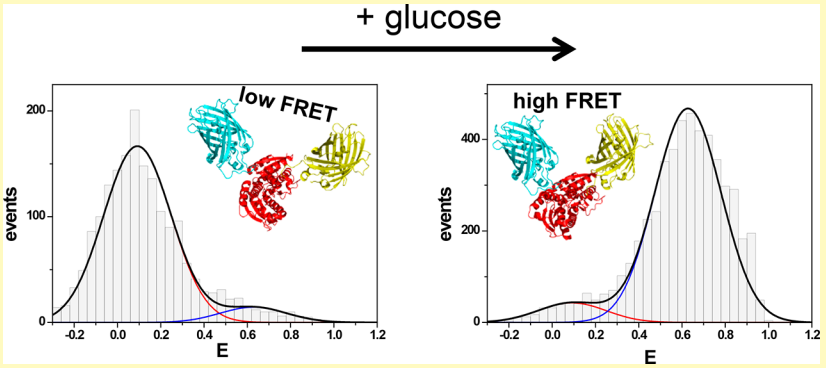

ABSTRACT: Genetically encoded Förster resonance energy transfer (FRET)-based biosensors for the quantification of ligand molecules change the magnitude of FRET between two fluorescent proteins upon binding a target metabolite. When highly sensitive sensors are being designed, extensive sensor optimization is essential. However, it is often difficult to verify the ideas of modifications made to a sensor during the sensor optimization process because of the limited information content of ensemble FRET measurements. In contrast, single-molecule detection provides detailed information and higher accuracy. Here, we investigated a set of glucose and crowding sensors on the single-molecule level. We report the first comprehensive single-molecule study of FRET-based biosensors with reasonable counting statistics and identify characteristics in the single-molecule FRET histograms that constitute fingerprints of sensor performance. Hence, our single-molecule approach extends the toolbox of methods aiming to understand and optimize the design of FRET-based biosensors.

KEYWORDS: *glucose sensor, crowding sensor, single-molecule FRET, conformational change, chomophore maturation*

Genetically encoded Förster resonance energy transfer (FRET)-based biosensors are powerful analytical tools that can for example recognize the presence of specific small molecules or sense environmental conditions in vivo.[1] The sensors are fusion proteins that consist of a central sensing protein flanked by two fluorescent proteins. The optical readout of the sensor is based on FRET between the fluorescent proteins that changes upon ligand binding to the sensing protein or because of other environmental impacts. There are various strategies for optimizing a sensor (i.e., increasing the change in FRET) concerning the central sensing protein, the fluorescent proteins (FPs), and the linker sequences between them.[1,2] However, a detailed molecular understanding of how a certain sensor modification affects FRET is lacking and is still an object of investigation.[3−5]

A frequently employed application of FRET-based biosensors is the detection of intracellular metabolites. Prototypical examples of these sensors are those based on periplasmic binding proteins (PBPs) as the ligand binding protein making use of the Venus flytrap principle.[6−8] According to Förster's theory, a substantial change of FRET is accomplished only if ligand binding alters the distance and/or the relative orientation between the chromophores of the FPs.[9,10] This can be achieved by modification of the polypeptide linkers that connect the FPs to the ligand binding protein. However, one reason for difficulties in achieving sufficient sensor performance is the limited information content of ensemble FRET data, which makes it hard to relate the impact of sensor modifications to the ideas that guide them.

Received: February 15, 2018
Accepted: July 6, 2018
Published: July 6, 2018

DOI: 10.1021/acssensors.8b00143
ACS Sens. 2018, 3, 1462−1470

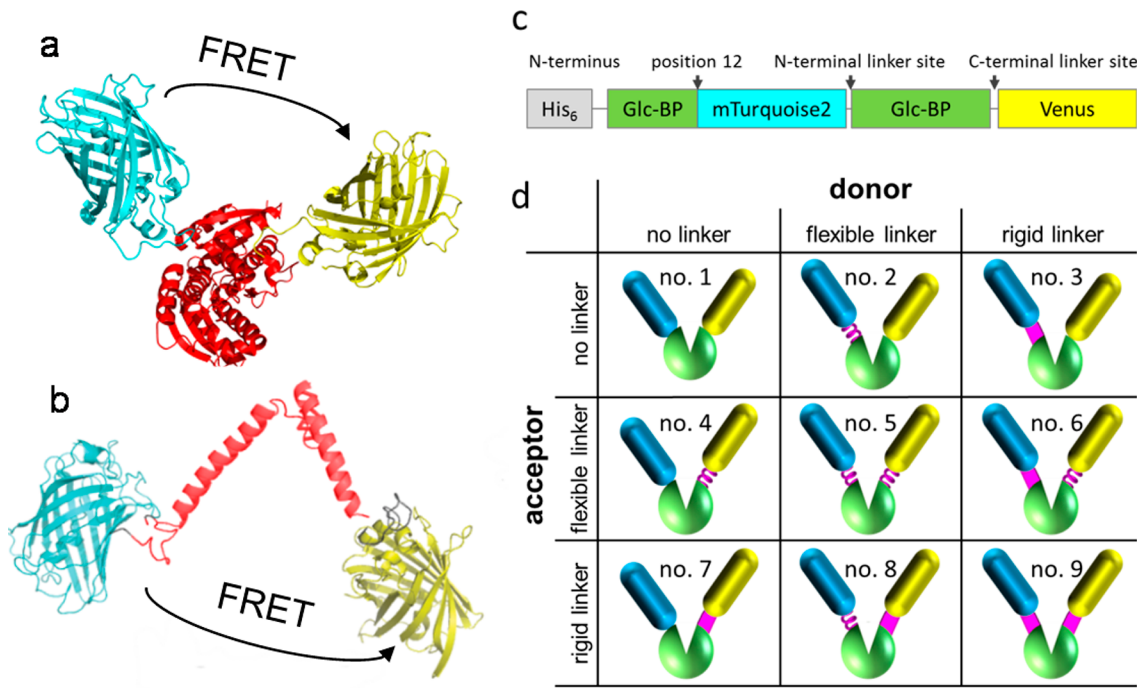

Figure 1. Graphical illustration of investigated biosensors. (a) Glucose sensor consisting of binding domain (red) equipped with donor (cyan) and acceptor (yellow) FPs. (b) Crowding sensor GE with linker domain (red) fused to donor (cyan) and acceptor (yellow) FPs. (c) Construction of the sensors composed of glucose-binding protein (Glc-BP), with inserted mTurquoise2 (donor) and Venus (acceptor). For N-terminal and C-terminal linkers, see linker toolbox (d) (no linkers, flexible linker, or rigid linker). (d) Sensor toolbox containing sensors without and with different linker combinations of flexible linkers, depicted as a purple helix, and stiff linkers, presented as a purple cylinder. All sensors carry additional amino acid sequences next to the central binding protein originating from restriction sites and an N-terminal His_6-tag (Table S1).

Therefore, in this contribution we present a new approach making use of single-molecule analysis to characterize different FRET-based sensors in more detail. Our approach benefits from the fact that single-molecule FRET (smFRET) can discriminate between coexisting conformational states in solution. Furthermore, the use of confocal multiparameter fluorescence detection delivers data of improved accuracy in determining the energy-transfer efficiencies and in resolving contributions from distinct population as compared to the usual ensemble measurements.[11] Thereby, we focus on sensors that use cyan and yellow FPs as a FRET pair. We demonstrate the potential of our approach by a comparative analysis of different variants of a glucose sensor which strongly vary with respect to their sensing performance. Furthermore, one glucose sensor variant and two recently developed specific crowding sensors[12] were investigated under crowding conditions. The related smFRET histograms exhibit a clearly different response to crowding as compared to glucose. In summary, each smFRET histogram displays a specific fingerprint of the respective sensor properties and elucidates the sensor's operating principles.

MATERIALS AND METHODS

Sensor Constructs. Construction of nine investigated glucose sensor constructs with different linker properties was performed as described by Steffen et al.[13] The design of the sensor prototype (no. 1) is based on the composition of the sensor FLII12Pglu 600μ,[9] with altered FP variants for improved fluorescent properties (see Figure 1). Furthermore, additional amino acids flanking the central binding protein were inserted as restriction sites necessary for the cloning strategy (see the Supporting Information Experimental Section for more details).

The studied crowding sensors consist of either an unstructured linker peptide with a length of 54 amino acid residues (G18) or a α-helical peptide linker with a total length of 118 residues (GE); the latter is shown in Figure 1b. In both cases these linker elements were sandwiched between a mCerulean3 donor and mCitrine acceptor. The sequences of the crowding sensor constructs G18 and GE can be found in ref 14. Further details on sensor production and sample preparation are given in the Supporting Information Experimental Section.

Methods. *Ensemble Fluorescence Measurements.* Isothermal binding curves of the glucose sensors were determined in a microtiter plate spectrofluorimeter as described earlier.[13] Per well, 50 μL of sensor solution was mixed each with 50 μL of 24 different glucose solutions (20 mM MOPS; pH 7.3; final glucose concentrations, 1 μM to 1.25 M). The ensemble characterization of a FRET-based biosensor (sensor concentration 1 μM) was performed by an intensity-based readout. Upon donor excitation (at 420 nm), the typical double-peaked fluorescence emission spectrum was observed with emission maxima at 472 nm for the donor (I_D) and 524 nm for the acceptor (I_A) (Figure S1a). The intensity ratio $R = I_A/I_D$ was plotted as a function of the glucose concentration [G] and fitted with a sigmoidal curve

$$R = (R_{max} - R_{apo})\frac{[G]}{K_D + [G]} + R_{apo} \quad (1)$$

where R_{apo} is the ratio without glucose, R_{max} the ratio at saturated glucose concentrations, and K_D the glucose concentration at which R increased to half its maximal rise (Figure S1b). A possible impact of donor-only fractions on R values and related E values was investigated in more detail as described in the Supporting Information Experimental Section (Figures S1d and S2). All graphs showing R values as a function of glucose or crowder concentrations are based on three replicate measurements if not stated differently.

Single-Molecule FRET Measurements. Major limitations for successful smFRET studies are caused by (i) photophysical drawbacks of the FPs, (ii) by a rather strong spectral overlap between donor and

DOI: 10.1021/acssensors.8b00143
ACS Sens. 2018, 3, 1462−1470

acceptor emission (Figure S3), and (iii) by a non-negligible direct acceptor excitation (Figure S4). At least two properties of our confocal microscope setup and the subsequent data analysis were crucial for the usability of the measured data: (i) concerning the excitation wavelength for the donor, the respective dichroic mirrors and emission filters were chosen such that the corresponding Raman scattering was excluded as far as possible from the fluorescence emission channel, and (ii) the use of pulsed interleaved excitation (PIE) was mandatory to eliminate donor-only contributions from the measured data.[15]

Measurements with diffusing sensor constructs were performed on a confocal microscope MicroTime 200 (PicoQuant, Berlin, Germany). Briefly, two pulsed diode lasers with emitting wavelengths of 437 nm (LDH-D-C-440, PicoQuant) and 509 nm (LDH-D-C-510, PicoQuant) were operated at a frequency of 20 MHz with an average emission power of 17 and 5 μW, respectively. In sample solutions with highly diluted sensor molecules (a few picomolar), one can obtain energy-transfer efficiencies for every single molecule by applying a burst analysis.[16,17] The measured time traces give access to photon bursts originating from single molecules appearing as dips in the interphoton lag and could be selected by a suitable threshold value.[18] For each selected burst, donor and acceptor photon counts (F_D, F_A) after donor excitation were accumulated and corrected. For burst with $F_D + F_A > 20$, we calculated the energy-transfer efficiency

$$E = \frac{F_A}{F_A + \gamma F_D} \quad (2)$$

for each burst. The determination of the correction factor γ was accomplished by plotting the inverse stoichiometry ($1/S$) versus E (see Figure S5b).[19] Because of the low molecular brightness of the involved FPs, we used a total measuring time of 8−10 h to obtain a few thousand up to a few tens of thousands of bursts for each sample condition. The corrected E values obtained for each burst were finally plotted on a histogram; depending on the number of available bursts, we chose 30−80 bins for the whole range of E values. By using the PIE excitation scheme, we were able to compare histograms including donor-only contributions and those where donor-only bursts were sorted out (Figure S6).

The obtained FRET histograms for glucose titrations were fitted globally with two Gaussian distributions (Figure S1c), and sensors at different crowding concentrations were fitted individually with one or two Gaussians. All data analysis was performed with self-written MATLAB (R2015b, 64-bit) scripts or using OriginPro (9.0.0G, 64bit). A more detailed description of all applied procedures is given in the Supporting Information Experimental Section.

RESULTS AND DISCUSSION

Ensemble versus Single-Molecule FRET Data. A crucial parameter for FRET-based sensors is given by the change between the minimal (R_{apo}) and the maximal (R_{max}) ratio, i.e., $\Delta R = R_{max} - R_{apo}$ (see eq 1 and Figure S1b). Maximizing this change (ΔR) is of the utmost importance when optimizing a FRET-based biosensor. Usually such measurements are performed with ensembles of sensor molecules, resulting in binding isotherms based on ensemble-averaged R values.[8,9] In contrast to ensemble data, single-molecule data can provide detailed information on coexisting sensor subpopulations, which in addition permits the discrimination of heterogeneities arising from experimental artifacts or impaired sample preparations.[11] In this respect also the degree of chromophore maturation of the individual fluorescent proteins (FPs) plays a critical role, because nonfluorescent donor or acceptor FPs lead to inoperable sensor molecules. Because of the limited molecular brightness (i.e., number of emitted photons per fluorophore molecule in a given time interval) of FPs compared to commercially available organic fluorescent dyes, reports on single-molecule FRET studies of FP-equipped biosensors are rare in the literature.[20,21] In addition, FPs are prone to photobleaching, which impedes single-molecule detection. However, as outlined in Materials and Methods and discussed in more detail in the Supporting Information Experimental Section, we managed to obtain reasonable single-molecule data from all sensor constructs.

As already mentioned, the ratio parameter R is typically utilized to quantify the performance of a specific sensor in ensemble studies. This parameter is well-suited to compare the response to different ligand concentrations of one and the same sensor. In order to compare the performances of different FRET-based sensors among each other, a parameter on an absolute scale, like the transfer efficiency E, is beneficial (see eq 2 in Materials and Methods for definition of E), because it can take values between 0 and 1. Compared to typical smFRET histograms measured with organic fluorescent dyes attached to the protein structure, we observed a pronounced broadening of the populations well beyond the shot noise limit (see example in Figure S1c).[22] In addition to triplet-state formation in the fluorophores or other fast blinking processes,[23] this is most probably caused by the fact that the FPs show a remaining translational and rotational mobility relative to the sensing domain on a time scale longer than the experimental observation time (i.e., a few milliseconds). In such a scenario, the sensing domain remains either in the nonliganded or in the liganded state, while in both states the slightly mobile FPs either change their relative chromophore orientation or alter their spatial distance.[21]

It is obvious that successful FRET measurements require two functional FPs. In practice, the degree of the chromophore maturation in the specific FP variant depends on several factors that can be different from one sensor construct to the other. Among others, the choice of the respective FP variant, the production by recombinant *Escherichia coli*, and the layout of a sensor construct might influence the maturation efficiency of the chromophores.[24] In particular, if the acceptor FP in a sensor molecule is nonfluorescent, the measured I_D value is artificially increased, and as a result the important ΔR value cannot reach its potential maximal value (Figure S1d). Therefore, knowing the value of the donor-only molecule fraction in a sensor population is crucial when evaluating the performance of a specific sensor construct. Single-molecule detection offers a unique possibility to quantify the donor-only fraction. An absorption measurement can obviously yield the total amount of fluorescent donors and acceptors in a sample. However, it cannot deliver a value for the donor-only fraction because the distribution of the FPs among the individual sensor molecules is not known. Hence, we exploited the dual-color excitation on the confocal microscope to make use of two-color coincidence detection.[25,26] This single-molecule approach enables discrimination between sensor molecules carrying two functional FPs and those which fluoresce at only one color (Figure S6). Of course, acceptor-only molecules also weaken the readout signal, because they do not contribute to the signal at all. However, in a FRET experiment, only donor molecules are directly excited, and accordingly, varying acceptor-only fractions do not change the value of the FRET readout itself, e.g., the FRET ratio R or transfer efficiency E.

Analysis of FRET-Based Glucose Sensors with Different Linkers. In order to demonstrate the capability of utilizing transfer efficiency histograms to evaluate the performance of FRET-based biosensors, we analyzed various glucose sensor constructs with a systematic variation of different linker

DOI: 10.1021/acssensors.8b00143
ACS Sens. 2018, 3, 1462−1470

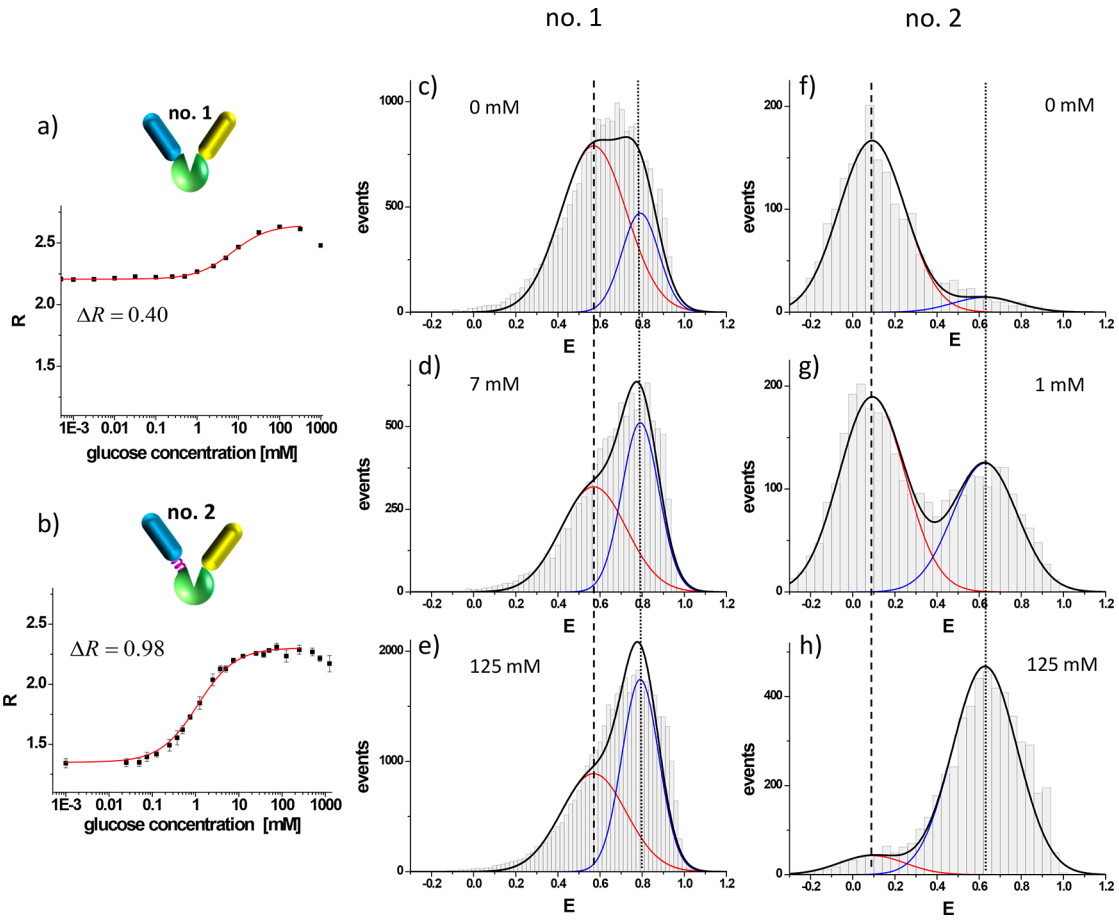

Figure 2. Ensemble characterization of construct no. 1 (a) and no. 2 (b) based on relative increase of FRET ratio parameter R supported by the corresponding glucose binding isotherm (red curve). FRET efficiency histograms (without donor-only contributions) at different glucose concentrations globally fitted with two Gaussians (same mean position and width for all glucose concentrations, but individual statistical weights for each population): without glucose (c, f), at K_D of binding isotherm (d, g), and at saturating glucose concentration of 125 mM (e, h). The difference in the mean position of both populations ($\Delta E_{pop} = E_2 - E_1$) shown by dashed ($E_1$) and dotted ($E_2$) vertical lines. For more details see the Supporting Information.

combinations between the glucose binding domain and the flanking FPs (see Figure 1c,d). A similar linker toolbox approach was recently used to vary the sensor properties of a FRET-based L-lysine sensor.[13] All glucose sensor constructs were characterized by binding isotherms (Figure S1b) recorded with a microtiter plate fluorimeter. Some of the applied linker modifications gave highly improved signal changes compared to the prototype sensor (see also a similar behavior for the L-lysine sensor[13]). Deeper insight was obtained by measuring three different FRET efficiency histograms: (i) in the absence of glucose, (ii) at a millimolar concentration of glucose (approximately at the K_D), and (iii) at 125 mM glucose with fully saturated sensor molecules. The obtained FRET efficiency histograms show typically two populations representing two states. Consequently, they were fitted globally with two Gaussians that had the same mean position and width for all glucose concentrations but individual statistical weights for each population (for details, see Supporting Information Experimental Section).

As a starting point, the sensor prototype (no. 1 in Figure 1d) was investigated. The prototype sensor showed only a modest signal change of $\Delta R = 0.40$ (Figure 2a). The smFRET histogram shows two strongly overlapping populations in the absence of glucose (see Figure 2c). Both populations are already centered at rather high mean transfer efficiencies (E_1 = 0.57 and E_2 = 0.79; see Table S2 for all fitting parameters). With increasing glucose concentration, the population at E_1 = 0.57 is depopulated by approximately one-third, while the other population at higher transfer efficiency increased its statistical weight accordingly. For this sensor construct, we could not observe significant differences between the histograms measured at K_D of 7 mM glucose concentration (Figure 2d) and at 125 mM (Figure 2e). In principle, we would have expected that the histogram for 7 mM (Figure 2d) shows a relation of the statistical weights for both populations which is between those found in panels c and e of Figure 2. However, a combination of effects originating from rather small ΔR values, forming a strong overlap of the involved populations in the histogram, and from the nonlinearity between R and E values gives rise to almost indistinguishable histograms for the K_D and the saturating concentration conditions in this case.

Next, we considered sensor no. 2, which showed the largest glucose-induced signal change of all investigated sensors (ΔR = 0.98, see Figure 2b). Here, the donor is connected via a flexible linker to the glucose binding protein. In the absence of glucose, we observed a dominant population (92% statistical weight) centered at a rather low transfer efficiency of E_1 = 0.09 that is well-separated from a much smaller population (8%) at a high transfer efficiency of E_2 = 0.63 (Figure 2f). With rising glucose concentration, the statistical weight of the low-FRET

DOI: 10.1021/acssensors.8b00143
ACS Sens. 2018, 3, 1462−1470

Table 1. Parameters Characterizing the Sensor Performance

sensor construct no.	ΔR[a]	$\Delta E_{avg,D0}$[b]	ΔE_{avg}	ΔE_{pop}[c]	$\Delta E_{avg,D0}/\Delta E_{pop}$[d]	$\Delta E_{avg}/\Delta E_{pop}$
1	0.40	0.040	0.066	0.221	18%	30%
2	0.98	0.302	0.467	0.536	56%	87%
3	0.92	0.268	0.390	0.468	57%	83%
4	0.22	0.135	0.183	0.305	44%	60%
5	0.49	0.224	0.313	0.394	57%	79%
8	0.52	0.088	0.133	0.293	30%	45%

[a] ΔR values characterize the sensor sensitivity at ensemble level. [b] $\Delta E_{avg,D0}$ represents the difference of the average FRET efficiency E between 0 and 125 mM glucose including the donor-only contribution with $\Delta E_{avg,D0} = (1 - x_{D0})\,\Delta E_{avg}$, where x_{D0} is the donor-only fraction (see Figure S9) and ΔE_{avg} is the difference between the average single-molecule E measured at 0 and 125 mM glucose without donor-only contributions ($\langle E \rangle_{sm}$ in Table S2). [c] ΔE_{pop} values give the difference between low-FRET (E_1) to the high-FRET (E_2) state. [d] The difference between $\Delta E_{avg,D0}/\Delta E_{pop}$ and $\Delta E_{avg}/\Delta E_{pop}$ enumerates the reduction in the sensor performance caused solely by donor-only fractions.

population decreased concomitant with an increase of the high-FRET population (Figure 2g). At saturating glucose concentration, the high-FRET population increased its statistical weight up to 91%, while only a small low-FRET population (9%) was left (Figure 2h and Table S2). According to the development of smFRET histograms upon increasing glucose concentrations, the most reasonable model assumption for the underlying mechanism is to assign the nonliganded (open) state to the low-FRET population and the fully liganded (closed) state to the high-FRET population. Obviously, the large difference in the performance of sensors no. 1 and no. 2 measured in ensemble (cf. Figure 2a,b) is reflected in a strong divergence between the corresponding smFRET histograms. We also measured smFRET histograms for some further sensor constructs.

In fact, the two sensors shown in Figure 2 display two extreme scenarios of possible sensor behavior. Other constructs obtained from the toolbox exhibited performances that are between the above-described extreme scenarios (see Figure S7). Based on the smFRET histograms of all investigated sensor constructs, mainly two conclusions seem to be essential to achieve the intended large signal change ΔR: (i) The nonliganded state should be accumulated in a population at low transfer efficiency in order to allow for a large ΔE with respect to the population of the liganded state at higher transfer efficiencies. (ii) Under ideal conditions, a preferably complete transfer of molecules from the low-FRET population toward the high-FRET population should take place with increasing ligand concentration. Both conditions are fulfilled to a large extent for the sensor construct no. 2. In contrast to this, the performance of the sensor prototype no. 1 is impaired: first, by a much smaller ΔE_{pop} between the low-FRET and high-FRET population and second, by an incomplete transfer of molecules from the low-FRET state toward the high-FRET state.

The major goal in designing highly sensitive sensors is to establish a robust conversion of a relative small ligand-induced conformational change within the glucose-binding protein into a measurable rearrangement of the FPs resulting in the highest possible ΔE. Here, single-molecule data provide valuable information on the extent to which this requirement is fulfilled. We can distinguish between scenarios with an insufficient translation mechanism (i.e., a small ΔE_{pop} between non-liganded and liganded states, Figure 2) and those in which in principle a reasonable conversion mechanism is established, but only a limited fraction of all sensor molecules makes use of it. In fact, often a combination of both problems was observed. From investigations of the sensor constructs investigated in this study, we learned that the linker between the N-terminal donor and the glucose binding protein is most important with the introduction of either a flexible or a rigid linker resulting in functional sensor constructs having the desired features (sensors no. 2 and no. 3, shown in Figures 2 and S7, respectively). By contrast, the additional introduction of a linker between the acceptor and the glucose binding protein (sensors no. 5 and no. 8) lowered the sensor performance, because a significant fraction of sensor molecules are already converted into the high-FRET state in the absence of glucose (Figure S7). The absence of linkers (sensor no. 1) or only a linker at the acceptor FP site (sensor no. 4) gave even weaker sensor performances. Because the remaining sensors produced with the linker-tool box approach (no. 6, no. 7, and no. 9) showed rather poor performance, we do not expect further insights from smFRET histograms and omitted therefore single-molecule studies for these constructs. For all six sensor constructs which we analyzed on single-molecule level, we also calculated averaged R values and compared them to the related values from the ensemble measurements. Within the limits of errors, this comparison revealed a reasonable consistency between ensemble and single-molecules measurements (see Figure S8).

The comparison of three different ΔE values in Table 1, calculated from the obtained smFRET histograms, allowed a stepwise identification and quantification of properties that reduced the sensor performance. First, the difference of the average transfer efficiency between 0 and 125 mM glucose is calculated, in one case by including the donor-only molecules ($\Delta E_{avg,D0}$) and in another case after sorting them out (ΔE_{avg}). Second, we quantify the difference between the mean positions of the low-FRET and high-FRET population (ΔE_{pop}). Finally, we give $\Delta E_{avg,D0}$ and ΔE_{avg} in relation to ΔE_{pop}, because ΔE_{pop} defines the ultimate limit for the specific sensor performance, i.e., all sensor molecules shift completely from the low-FRET to the high-FRET state. The higher the value of ΔE_{pop}, the better the conversion of the glucose-induced conformational change into a change in FRET efficiency. How efficient the sensor construct makes use of this conversion, i.e., which fraction of the sensor molecules changes from the low-FRET to the high-FRET state, is given by $\Delta E_{avg}/\Delta E_{pop}$. Here, the sensor constructs no. 2 and no. 3 show the highest ΔE_{pop}, and a large fraction of the molecules makes use of the transition (87% and 83%, respectively). Sensors nos. 4, 5, and 8 show intermediate ΔE_{pop} values, and a lower fraction of molecules take part in the transition (between 45% and 79%). At last, we estimated how large the change in FRET efficiency would be, if donor-only molecules could not be excluded (like in ensemble

DOI: 10.1021/acssensors.8b00143
ACS Sens. 2018, 3, 1462−1470

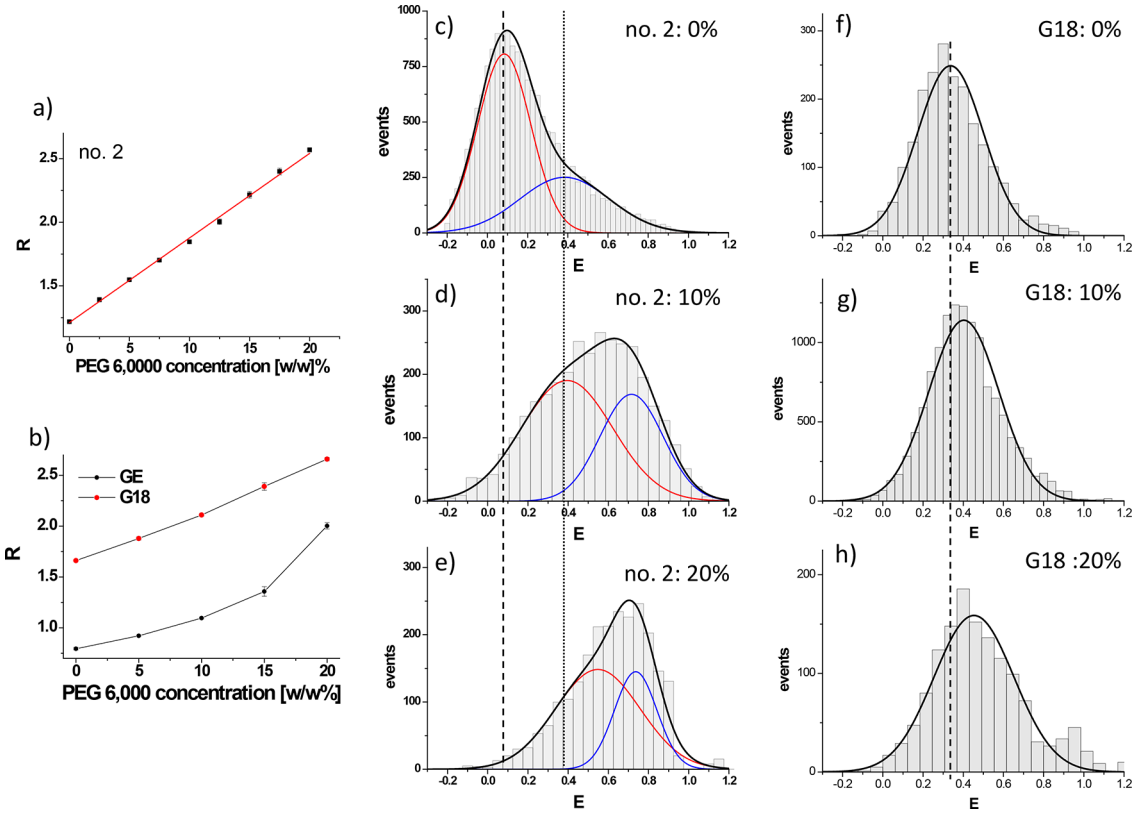

Figure 3. Ensemble fluorescence intensity ratio *R* for glucose sensor no. 2 (a) and for crowding sensors G18, GE (b) for different PEG 6000 concentrations. smFRET efficiency histograms of sensor no. 2 for increasing PEG 6000 concentrations fitted individually with two populations (c–e). A clear shift of the population means with increasing crowder concentration is observed, which is visualized by vertical reference lines positioned at the low-FRET peak (dashed) and at the high-FRET peak (dotted) as referenced for noncrowding conditions (i.e., 0%). smFRET efficiency histograms obtained for G18 sensor were fitted with a single Gaussian (f–h). All parameters obtained from the histogram fitting are given in Tables S2 and S3.

measurements), based on the donor-only fraction given in Figure S9. Because the glucose sensor constructs have a donor-only fraction in the order of 30–40%, we likewise observed a corresponding reduction of their potential FRET change. As mentioned already, *R* and *E* values are in general not proportional to each other, and a comparison between both is not straightforward. This is also indicated by the fact that the absolute value of *E* is crucial for the ensemble readout in terms of *R* values. On the one hand, the impact of errors on *R* due to varying donor-only fractions is much weaker, if the absolute values of *E* are small (see the Supporting Information Experimental Section). On the other hand, the sensitivity (given in Table 1 as ΔR) is much higher for larger absolute *E* values, because of the nonlinear relationship between *R* values and transfer efficiencies *E* (Figure S2b). This is demonstrated by comparison of sensors no. 1 and no. 4. The $\Delta E_{\mathrm{avg,D0}}$ of construct no. 4 is approximately 3-fold higher as compared to that of construct no. 1. However, the ΔR value of construct no. 4 is by a factor of 2 smaller as compared to that of construct no. 1, because the latter works on higher absolute values of *E* (cf. Table S2).

In summary, an ideal sensor would display (i) a low donor-only fraction (efficient acceptor maturation), (ii) a large difference in FRET efficiency between population means of nonliganded and liganded state, and finally (iii) a complete transfer from the low-FRET population (nonliganded) to the high-FRET population (liganded). At this time we do not really understand the molecular mechanisms which lead to the fact that a certain fraction of sensors shows already (closed) high-FRET states in the absence of glucose and why not all sensor molecules adopt the high-FRET state at saturating glucose concentrations. Although some of the investigated sensor constructs show already a quite reasonable performance (sensor nos. 2 and 3), there is additional potential to improve the sensors further, for example by employing circularly permuted FPs.[4,27]

Impact of Crowding Effects on FRET-Based Sensors. Because genetically encoded FRET-based biosensors are often employed in the crowded environment of the cytosol, we make use of the single-molecule approach to elucidate how molecular crowding affects such sensors. As known from previous studies, high concentrations of crowding agents have the potential to compact biological macromolecules.[28,29] This behavior was also observed for FRET-based biosensors, ffor example, promoted by synthetic macromolecular crowding agents that produced more compact conformations of the sensor caused by excluded volume effects.[30] However, this effect is typically undesired for metabolite sensors, because it impedes the usability of an in vitro calibration for data measured in vivo. In contrast, FRET-based biosensors were recently developed that specifically sense macromolecular crowding.[12,31] These sensors can potentially map how crowded certain compartments of the cell are and thereby provide insight into how crowding influences cellular processes. Here we investigated the effect of artificial crowding caused by

DOI: 10.1021/acssensors.8b00143
ACS Sens. 2018, 3, 1462–1470

polyethylene glycol (PEG) on glucose sensor no. 2 and on two crowding sensors.

The studied crowding sensors consist of either an unstructured linker peptide with a length of 54 amino acid residues (G18) or a α-helical peptide linker with a total length of 118 residues (GE) (Figure 1b). All sensors were titrated with the PEG 6000 (molecular mass of 6 kDa) up to concentrations of 20% (w/w). The resulting response to PEG 6000 for both the glucose and the crowding sensors, in terms of I_A/I_D, is shown in Figure 3a,b. Earlier studies on crowding sensors gave similar results.[12,31] The smFRET efficiency histograms of glucose sensor no. 2 in the presence of increasing PEG 6000 concentrations are displayed in Figure 3c–e. The measured distribution of FRET efficiencies were fitted again with two populations, as in the case of glucose titrations (Figure 2). The experimental data shown in Figures 2f and in 3c (both sensor no. 2) were measured under the same environmental conditions, but the sample analyzed in Figure 3c exhibits a more pronounced shoulder at larger E values. This is caused by varying sample properties or qualities of sensors from different sample batches and is not due to the measuring process itself. Different samples from one and the same batch exhibit a rather high reproducibility, as shown in Figure S10.

Also upon increasing crowder concentration, the FRET efficiency histograms are best fitted using a two-state model because the histograms exhibit a rather broad single-peaked but asymmetric distribution, which can only be fitted reasonable well with two components. Essentially, the two populations show an increasing overlap and a pronounced shift to larger E values in contrast to glucose titrations, where the histograms were best described by fixed population positions (see Figure S11 for comparison of different fitting approaches). This is a clear difference from the behavior of the above-described effects due to glucose binding where the population peak positions do not alter, but the relative occupancies of the respective populations do change. However, both additives (glucose and PEG) cause a structural compaction of the sensor constructs, but this is obviously driven by different molecular mechanisms. According to this observation, glucose binding is related to a conformational selection model in which equilibrium of at least two states preexists of which at least one state is able to bind glucose. Interestingly, rather high crowder concentrations led to even higher transfer efficiency values (E) compared to saturating glucose concentrations (cf. Figures 2h and 3e). However, even under conditions of relatively strong crowding, further addition of glucose leads to an increase of FRET (see Figure S12).

In contrast to the glucose sensors, the smFRET histograms of both crowding sensors show clearly a single population in aqueous buffer solutions (Figures 3f–h and S13b–d). Crowding sensors with increased crowder concentration resulted in FRET efficiency histograms with pronounced shifts of the population mean but still no appearance of a second population. Altogether, these observations lead to the conclusion that the crowding sensors do not show distinct long-lived states but most probably display an ensemble of different conformations. Increased crowder concentrations generate sensors with more compact conformations, which led to a continuous shift of the population to higher transfer efficiencies. However, they seem not to reach a defined saturating state at high crowder concentrations.[14] A similar crowder-induced peak shift was already observed earlier in smFRET studies on several dye-labeled intrinsically disordered proteins.[29] In summary, our single-molecule data reveals that the response mechanisms to crowding are rather similar for both types of sensors. Compared to the G18 and GE crowding sensors, the glucose sensor no. 2 seems to be even more sensitive in the regime of low crowder concentrations (i.e., below 10% (w/w) PEG 6000; Figure S13a). Unfortunately, a direct application of the glucose sensor as a crowding sensor in the cytosol is not straightforward, because metabolites in the cytosol like glucose would bias the readout of crowding.[30] On the other hand, an in vivo application of the glucose sensors, which is typically performed in a crowded environment of the cytosol, would need a crowding-adapted calibration of sensors in order to deliver reliable ligand concentration from the sensor readout. However, further improved crowding sensors may, for example, exhibit multiple states which populate or depopulate as a function of crowding. Here, our single-molecule approach can contribute to identifying or validating the targeted properties.

CONCLUSION

The aim of this study was to elucidate properties and functionalities of genetically encoded FRET-based biosensors in more detail by employing single-molecule spectroscopy. To date, smFRET studies on these sensors have not been performed on a quantitative level, mainly because of photophysical drawbacks of fluorescent proteins. Another difficulty with cyan (CFP) and yellow (YFP) fluorescent proteins (and derivatives thereof) utilized as FRET pairs is given by a strong spectral cross-talk and non-negligible direct YFP excitation. However, by employing state-of-the-art data acquisition and analysis, as well as long measuring times, we obtained meaningful FRET efficiency histograms, even in the presence of high concentrations of macromolecular crowding agents. We obtained a reasonable number of useful bursts which is still about 10-fold lower as compared to conventional smFRET studies with organic fluorescent dyes for the same data acquisition time.

Our single-molecule approach allows for identifying limiting factors that inhibit a good (glucose) sensor performance. It thereby offers possible starting points to improve the performance or may reveal that the sensor has almost reached its full performance. Although our data cannot provide a protocol detailing how the linkers should be modified to improve the sensor, it nevertheless provides valuable indications. For example, a FRET efficiency histogram of a glucose sensor that shows a large distance between its population centers (ΔE_{pop}) but only a small fraction of the molecules transfering between the populations might indicate that the conformational change is partly hindered. A minor linker modification, e.g., an extension, might in this case improve the sensor performance. In contrast, a sensor with a weak signal change but making use of the full population transfer might need a complete revision of the sensor design, e.g., by changing the insertion positions of the fluorescent proteins. Furthermore, single-molecule detection allows for excluding the donor-only bias from the data and even for quantifying the donor-only fractions. We observed significant differences between the donor-only fractions among the tested glucose sensors, but also between the glucose sensors and the crowding sensors. This information can also be used to guide sensor design. Of course, chromophore maturation is a complex interplay of environmental parameters that the

DOI: 10.1021/acssensors.8b00143
ACS Sens. 2018, 3, 1462–1470

fluorescent proteins encounter. However, in particular, improved YFP variants might increase the maturation efficiency and reduce the donor-only fraction. Although single-molecule FRET data is much less biased by experimental artifacts compared to ensemble data, a detailed discrimination between rotational movements and relative translational distance changes between the fluorescent proteins is still not straightforward. This knowledge would indeed give an important additional impact on a more targeted sensor design. Thus, we propose a combination of smFRET, small-angle X-ray scattering (SAXS),[32] and computational modeling[33,34] as the most promising approach to achieve further progress.

Finally, we note that the strength of our approach is given by the ability to characterize the performance of FRET sensors by employing smFRET. As a prerequisite, highly diluted samples in pure buffers (or with pure ingredients like PEG crowders) and rather long measuring times are required. Therefore, routine measurements of these sensors in physiological environments, like in cell culture supernatants or directly in cells, typically performed with microtiter plate readers or by fluorescence lifetime imaging measurements, are so far not a targeted application of our approach.

■ ASSOCIATED CONTENT

Supporting Information

The Supporting Information is available free of charge on the ACS Publications website at DOI: 10.1021/acssensors.8b00143.

Experimental Section; additional method details, figures, and tables (PDF)

■ AUTHOR INFORMATION

Corresponding Author

*E-mail: fitter@physik.rwth-aachen.de. Tel.: +49 241 80 27209. Fax: +49 241 80 22331.

ORCID

Arnold J. Boersma: 0000-0002-3714-5938

Jörg Fitter: 0000-0002-4503-2079

Author Contributions

J.F., H.H., M.P., and A.J.B. designed the research; H.H., J.O., and V.S. performed the research; M.P., V.S., J.O., and A.J.B. developed sensor constructs; H.H. analyzed the data, and H.H. and J.F. wrote the manuscript in consultation with all authors.

Notes

The authors declare no competing financial interest.

■ ACKNOWLEDGMENTS

The authors thank Drs. M. Gabba and M. Cerminara for initial support with the installation of the lasers, as well as Dr. J. Walter for preparing illustrations for Figure 1. H.H. acknowledges the International Helmholtz Research School of Biophysics and Soft Matter (BioSoft) for financial support. A.J.B. would like to acknowledge the Netherlands Organization for Scientific Research (NWO) for the Vidi grant (723.015.002).

■ REFERENCES

(1) Sanford, L.; Palmer, A. Recent Advances in Development of Genetically Encoded Fluorescent Sensors. *Methods Enzymol.* **2017**, *589*, 1−49.

(2) Okumoto, S.; Jones, A.; Frommer, W. B. Quantitative Imaging with Fluorescent Biosensors. *Annu. Rev. Plant Biol.* **2012**, *63*, 663−706.

(3) Komatsu, N.; Aoki, K.; Yamada, M.; Yukinaga, H.; Fujita, Y.; Kamioka, Y.; Matsuda, M. Development of an optimized backbone of FRET biosensors for kinases and GTPases. *Mol. Biol. Cell* **2011**, *22*, 4647−56.

(4) Ohta, Y.; Kamagata, T.; Mukai, A.; Takada, S.; Nagai, T.; Horikawa, K. Nontrivial Effect of the Color-Exchange of a Donor/Acceptor Pair in the Engineering of Forster Resonance Energy Transfer (FRET)-Based Indicators. *ACS Chem. Biol.* **2016**, *11*, 1816−22.

(5) Ast, C.; Foret, J.; Oltrogge, L. M.; De Michele, R.; Kleist, T. J.; Ho, C. H.; Frommer, W. B. Ratiometric Matryoshka biosensors from a nested cassette of green- and orange-emitting fluorescent proteins. *Nat. Commun.* **2017**, *8*, 431.

(6) de Lorimier, R. M.; Smith, J. J.; Dwyer, M. A.; Looger, L. L.; Sali, K. M.; Paavola, C. D.; Rizk, S. S.; Sadigov, S.; Conrad, D. W.; Loew, L.; Hellinga, H. W. Construction of a fluorescent biosensor family. *Protein Sci.* **2002**, *11*, 2655−75.

(7) Dwyer, M. A.; Hellinga, H. W. Periplasmic binding proteins: a versatile superfamily for protein engineering. *Curr. Opin. Struct. Biol.* **2004**, *14*, 495−504.

(8) Moussa, R.; Baierl, A.; Steffen, V.; Kubitzki, T.; Wiechert, W.; Pohl, M. An evaluation of genetically encoded FRET-based biosensors for quantitative metabolite analyses in vivo. *J. Biotechnol.* **2014**, *191*, 250−259.

(9) Deuschle, K.; Okumoto, S.; Fehr, M.; Looger, L. L.; Kozhukh, L.; Frommer, W. B. Construction and optimization of a family of genetically encoded metabolite sensors by semirational protein engineering. *Protein Sci.* **2005**, *14*, 2304−2314.

(10) Campbell, R. E. Fluorescent-protein-based biosensors: modulation of energy transfer as a design principle. *Anal. Chem.* **2009**, *81*, 5972−9.

(11) Sisamakis, E.; Valeri, A.; Kalinin, S.; Rothwell, P. J.; Seidel, C. A. Accurate single-molecule FRET studies using multiparameter fluorescence detection. *Methods Enzymol.* **2010**, *475*, 455−514.

(12) Boersma, A. J.; Zuhorn, I. S.; Poolman, B. A sensor for quantification of macromolecular crowding in living cells. *Nat. Methods* **2015**, *12*, 227.

(13) Steffen, V.; Otten, J.; Engelmann, S.; Radek, A.; Limberg, M.; Koenig, B. W.; Noack, S.; Wiechert, W.; Pohl, M. A Toolbox of Genetically Encoded FRET-Based Biosensors for Rapid L-Lysine Analysis. *Sensors* **2016**, *16*, 1604.

(14) Liu, B. Q.; Aberg, C.; van Eerden, F. J.; Marrink, S. J.; Poolman, B.; Boersma, A. J. Design and Properties of Genetically Encoded Probes for Sensing Macromolecular Crowding. *Biophys. J.* **2017**, *112*, 1929−1939.

(15) Muller, B. K.; Zaychikov, E.; Brauchle, C.; Lamb, D. C. Pulsed interleaved excitation. *Biophys. J.* **2005**, *89*, 3508−3522.

(16) Eggeling, C.; Berger, S.; Brand, L.; Fries, J. R.; Schaffer, J.; Volkmer, A.; Seidel, C. A. M. Data registration and selective single-molecule analysis using multi-parameter fluorescence detection. *J. Biotechnol.* **2001**, *86*, 163−180.

(17) Deniz, A. A.; Laurence, T. A.; Dahan, M.; Chemla, D. S.; Schultz, P. G.; Weiss, S. Ratiometric single-molecule studies of freely diffusing biomolecules. *Annu. Rev. Phys. Chem.* **2001**, *52*, 233−253.

(18) Fries, J. R.; Brand, L.; Eggeling, C.; Kollner, M.; Seidel, C. A. M. Quantitative identification of different single molecules by selective time-resolved confocal fluorescence spectroscopy. *J. Phys. Chem. A* **1998**, *102*, 6601−6613.

(19) Kudryavtsev, V.; Sikor, M.; Kalinin, S.; Mokranjac, D.; Seidel, C. A. M.; Lamb, D. C. Combining MFD and PIE for Accurate Single-Pair Forster Resonance Energy Transfer Measurements. *ChemPhysChem* **2012**, *13*, 1060−1078.

(20) Brasselet, S.; Peterman, E. J. G.; Miyawaki, A.; Moerner, W. E. Single-molecule fluorescence resonant energy transfer in calcium concentration dependent cameleon. *J. Phys. Chem. B* **2000**, *104*, 3676−3682.

DOI: 10.1021/acssensors.8b00143
ACS Sens. 2018, 3, 1462−1470

(21) Kyrychenko, A.; Rodnin, M. V.; Ghatak, C.; Ladokhin, A. S. Joint refinement of FRET measurements using spectroscopic and computational tools. *Anal. Biochem.* **2017**, *522*, 1−9.
(22) Nir, E.; Michalet, X.; Hamadani, K. M.; Laurence, T. A.; Neuhauser, D.; Kovchegov, Y.; Weiss, S. Shot-noise limited single-molecule FRET histograms: comparison between theory and experiments. *J. Phys. Chem. B* **2006**, *110*, 22103−22124.
(23) Kalinin, S.; Sisamakis, E.; Magennis, S. W.; Felekyan, S.; Seidel, C. A. On the origin of broadening of single-molecule FRET efficiency distributions beyond shot noise limits. *J. Phys. Chem. B* **2010**, *114*, 6197−6206.
(24) Newman, R. H.; Fosbrink, M. D.; Zhang, J. Genetically Encodable Fluorescent Biosensors for Tracking Signaling Dynamics in Living Cells. *Chem. Rev.* **2011**, *111*, 3614−3666.
(25) Li, H. T.; Ying, L. M.; Green, J. J.; Balasubramanian, S.; Klenerman, D. Ultrasensitive coincidence fluorescence detection of single DNA molecules. *Anal. Chem.* **2003**, *75*, 1664−1670.
(26) Kempf, N.; Remes, C.; Ledesch, R.; Zuchner, T.; Hofig, H.; Ritter, I.; Katranidis, A.; Fitter, J. A Novel Method to Evaluate Ribosomal Performance in Cell-Free Protein Synthesis Systems. *Sci. Rep.* **2017**, *7*, 467535.
(27) Baird, G. S.; Zacharias, D. A.; Tsien, R. Y. Circular permutation and receptor insertion within green fluorescent proteins. *Proc. Natl. Acad. Sci. U. S. A.* **1999**, *96*, 11241−6.
(28) Dhar, A.; Samiotakis, A.; Ebbinghaus, S.; Nienhaus, L.; Homouz, D.; Gruebele, M.; Cheung, M. S. Structure, function, and folding of phosphoglycerate kinase are strongly perturbed by macromolecular crowding. *Proc. Natl. Acad. Sci. U. S. A.* **2010**, *107*, 17586−91.
(29) Soranno, A.; Koenig, I.; Borgia, M. B.; Hofmann, H.; Zosel, F.; Nettels, D.; Schuler, B. Single-molecule spectroscopy reveals polymer effects of disordered proteins in crowded environments. *Proc. Natl. Acad. Sci. U. S. A.* **2014**, *111*, 4874−4879.
(30) Groen, J.; Foschepoth, D.; te Brinke, E.; Boersma, A. J.; Imamura, H.; Rivas, G.; Heus, H. A.; Huck, W. T. S. Associative Interactions in Crowded Solutions of Biopolymers Counteract Depletion Effects. *J. Am. Chem. Soc.* **2015**, *137*, 13041−13048.
(31) Gnutt, D.; Gao, M.; Brylski, O.; Heyden, M.; Ebbinghaus, S. Excluded-Volume Effects in Living Cells. *Angew. Chem., Int. Ed.* **2015**, *54*, 2548−2551.
(32) Mertens, H. D. T.; Piljic, A.; Schultz, C.; Svergun, D. I. Conformational analysis of a genetically encoded FRET biosensor by SAXS. *Biophys. J.* **2012**, *102*, 2866−75.
(33) Pham, E.; Chiang, J.; Li, I.; Shum, W.; Truong, K. A computational tool for designing FRET protein biosensors by rigid-body sampling of their conformational space. *Structure* **2007**, *15*, 515−23.
(34) Reinartz, I.; Sinner, C.; Nettels, D.; Stucki-Buchli, B.; Stockmar, F.; Panek, P. T.; Jacob, C. R.; Nienhaus, G. U.; Schuler, B.; Schug, A. Simulation of FRET dyes allows quantitative comparison against experimental data. *J. Chem. Phys.* **2018**, *148*, 123321.

DOI: 10.1021/acssensors.8b00143
ACS Sens. 2018, 3, 1462−1470